OPEN ACCESS

Type 2 inflammation promotes distinct metabolic profiles in chronic rhinosinusitis with nasal polyps

Takaaki Yonaga[1], Hiroki Ishii[1], Kentaro Yoshimura[2], Ayumi Shimamura[1], Kaname Sakamoto[1], Tomokazu Matsuoka[1], Daiju Sakurai[1]

[1] Department of Otolaryngology, Head and Neck Surgery, Interdisciplinary Graduate School of Medical Science, University of Yamanashi, Chuo, Japan

[2] Division of Molecular Biology, Center for Medical Education and Sciences, Interdisciplinary Graduate School of Medicine, University of Yamanashi, Chuo, Japan

Rhinology 64: 3, 0 - 0, 2026
https://doi.org/10.4193/Rhin25.540

Received for publication:
September 24, 2025
Accepted: February 2, 2026

Associate Editor:
Michael Soyka

Dear Editor:

Chronic rhinosinusitis (CRS) is an inflammatory disorder of the sinonasal mucosa that occurs with or without nasal polyps (NPs). Compared with CRS without NPs, CRS with NPs (CRSwNP) is associated with more severe and uncontrolled sinonasal symptoms [(1)]. Type 2 inflammation, driven by T_{H2} cytokines (interleukins 4, 5, and 13), promotes eosinophilic infiltration into NPs and contributes to disease progression and recurrence [(2)]. Although recent studies have emphasized biological phenotyping and identified genetic/epigenetic endotypes to optimize treatment strategies for CRSwNP [(3)], clinical translation remains limited. Because cellular phenotypes are strongly influenced by metabolic alterations [(4)], profiling of the metabolic landscape may provide insight into CRSwNP pathogenesis and identify biomarkers of type 2 inflammation–related symptom exacerbation, treatment resistance, and recurrence. However, metabolomic characterization of CRSwNP remains underexplored.

To address this gap, we performed liquid chromatography/electrospray ionization–mass spectrometry–based quantitative analysis on paired inferior turbinate (IT) and NP tissues from 13 patients with CRSwNP, identifying 38 metabolites (Table S1, Figure 1A). Correlation analysis revealed coordinated metabolic changes in NPs (Figure S1A). Among these metabolites, glutamic acid (area under the curve [AUC]: 0.9048, $p = 0.0152$) and kynurenine (AUC: 0.8333, $p = 0.0455$), which were decreased and increased in NPs compared with ITs, respectively, were associated with early recurrence within 6 months after surgery (Figure 1B, Figure S1B, C). Pathway enrichment analysis indicated suppression of the tricarboxylic acid (TCA) cycle via reduced glutamic acid and branched-chain amino acids (BCAAs), with a metabolic bottleneck at succinic acid–to–fumaric acid conversion, resulting in two-fold higher succinic acid accumulation in NPs (Figure 1C, Figure S1D–F). Kynurenine accumulation further suggested impaired kynurenine catabolism in NPs (Figure 1C).

To complement these findings, we integrated publicly available single-cell transcriptomic data from IT and NP tissues of patients with CRSwNP. Among 13 major cell clusters, basal cells—the predominant population in CRSwNP—exhibited cell-type–specific downregulation of the identified metabolic pathways (Figure 1D, Figure S2A–D). Genes related to the TCA cycle (SDHA, FH, MDH2), glutamic acid metabolism (GLS, GLUL, GLUD1), and kynurenine catabolism (KYNU) were significantly downregulated in basal cells (Figure S2E). Correlation analysis revealed a negative association between TSLP expression and glutamic acid–dependent reductive TCA cycle gene expressions in basal cells (Figure 1E).

Glutamic acid supports cellular energy production through the reductive TCA cycle under oxidative stress [(5)]. Because type 2 inflammation is associated with increased oxidative stress in NPs of patients with CRSwNP, enhanced glutamic acid consumption may reflect a metabolic consequence of the inflammatory microenvironment. Succinic acid accumulation may further contribute to eosinophilic inflammation because succinate promotes eosinophil recruitment and retention [(6)]. Kynurenine, derived from tryptophan metabolism, is implicated in type 2 inflammation, and impaired tryptophan–kynurenine metabolism exacerbates bronchial asthma [(7)]. Moreover, dysregulation of coagulation and fibrinolytic systems contributes to CRSwNP pathogenesis [(2)], and elevated kynurenine levels have been linked to coagulation activation [(8)]. Thus, impaired kynurenine catabolism may represent a metabolic alteration associated with fibrinolytic and coagulation pathway activation in NPs. A subset of basal cells in CRSwNP responds to type 2 cytokines by undergoing hyperplasia and producing thymic stromal lymphopoietin (TSLP), a danger signal that amplifies local type 2 inflammation [(9)]. Collectively, these findings support a link between metabolic alterations in basal cells and TSLP production in NPs, although mechanistic validation is required.

Despite limitations including the small cohort size and short follow-up period, our integrative omics analyses demonstrate

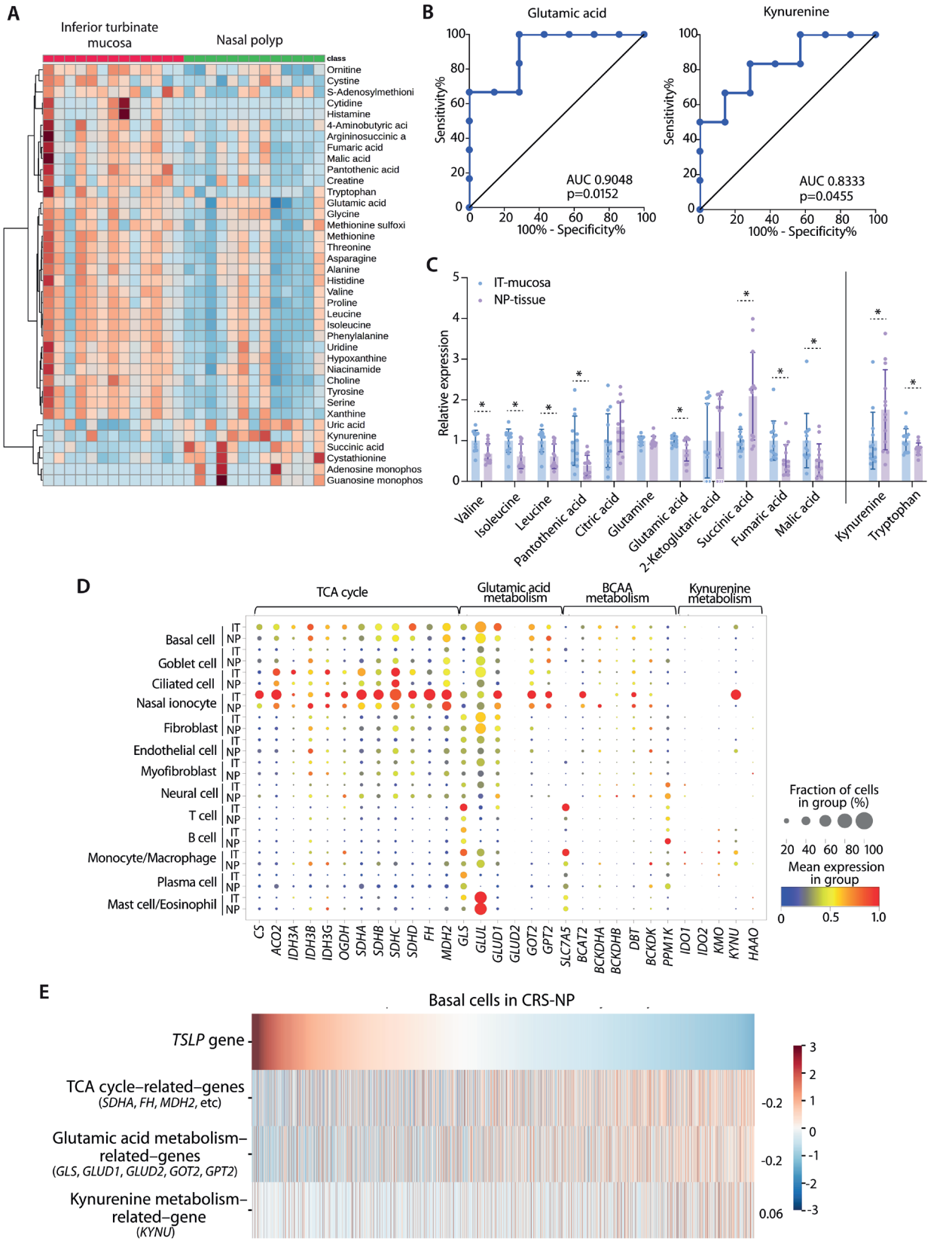

Figure 1. Metabolic reprogramming in NPs of patients with CRSwNP. (A) Heatmap of differentially expressed primary metabolites between paired IT and NP tissues. (B) Receiver operating characteristic curves for glutamic acid and kynurenine in predicting early recurrence. (C) Relative levels of TCA cycle intermediates, BCAAs, and kynurenine metabolism in ITs and NPs. *p < 0.05. (D) Dot plot of gene expression in metabolic pathways, including the TCA cycle, glutamic acid and BCAA metabolism, and kynurenine catabolism, across annotated cell clusters in ITs and NPs. (E) Heatmap of TSLP expression and corresponding metabolic pathway scores in basal cells from NPs, with Spearman's ρ values shown.

reduced glutamic acid and BCAAs, TCA cycle dysregulation with succinate accumulation, and impaired kynurenine catabolism in CRSwNP, highlighting metabolic reprogramming as a potential therapeutic target.

Acknowledgment

We are grateful to A. Manita for providing technical assistance.

Authorship contributions

TY, HI and DS conceived the study design. TY, HI and KY conducted the experiments. TY and TM collected tissue samples from patients with eosinophilic CRS. TY, AS, KS and HI analyzed and interpreted the data. TY and HI wrote the initial manuscript draft. TY, HI and DS performed critical editing. All authors approved the final version of the manuscript.

List of abbreviations

AUC: area under the curve; BCAA(s): branched-chain amino acid(s); CRS: chronic rhinosinusitis; CRSwNP: chronic rhinosinusitis with nasal polyps; IT(s): inferior turbinate(s); NP(s): nasal polyp(s); TCA: tricarboxylic acid; TSLP: thymic stromal lymphopoietin.

Conflict of interest

The authors have no conflicts of interest to declare.

Funding

This work was supported by Grants-in-Aid for Scientific Research from the Japan Society for the Promotion of Science (JSPS) (KAKENHI grant numbers 21K16828, 22K09740, and 23K08959 to KS, DS and HI).

References

1. Fujieda S, Imoto Y, Kato Y, et al. Eosinophilic chronic rhinosinusitis. Allergol Int. 2019;68(4):403-12.
2. Takabayashi T, Schleimer RP. Formation of nasal polyps: the roles of innate type 2 inflammation and deposition of fibrin. J Allergy Clin Immunol. 2020;145(3):740-50.
3. Tomassen P, Vandeplas G, Van Zele T, et al. Inflammatory endotypes of chronic rhinosinusitis based on cluster analysis of biomarkers. J Allergy Clin Immunol. 2016;137(5):1449-56 e4.
4. Zhang A, Sun H, Xu H, Qiu S, Wang X. Cell metabolomics. OMICS. 2013;17(10):495-501.
5. Metallo CM, Gameiro PA, Bell EL, et al. Reductive glutamine metabolism by IDH1 mediates lipogenesis under hypoxia. Nature. 2011;481(7381):380-4.
6. Tannahill GM, Curtis AM, Adamik J, et al. Succinate is an inflammatory signal that induces IL-1beta through HIF-1alpha. Nature. 2013;496(7444):238-42.
7. Miao Y, Zhong C, Bao S, et al. Impaired tryptophan metabolism by type 2 inflammation in epithelium worsening asthma. iScience. 2024;27(6):109923.
8. Pawlak K, Mysliwiec M, Pawlak D. Hypercoagulability is independently associated with kynurenine pathway activation in dialysed uraemic patients. Thromb Haemost. 2009;102(1):49-55.
9. Kawakita K, Kouzaki H, Murao T, et al. Role of basal cells in nasal polyp epithelium in the pathophysiology of eosinophilic chronic rhinosinusitis (eCRS). Allergol Int. 2024;73(4):563-72.

Hiroki Ishii
Department of Otolaryngology
Head and Neck Surgery
Interdisciplinary Graduate School of
Medical Science
University of Yamanashi
1110 Shimokato
Chuo
Yamanashi 409-3898
Japan

Tel: +81-55-273-1111
E-mail: ishiih@yamanashi.ac.jp

This manuscript contains online supplementary material

SUPPLEMENTARY MATERIAL

Materials and Methods

Biological samples

This study was conducted in accordance with the Declaration of Helsinki and was performed using methods approved by the Ethics Committee of the University of Yamanashi (No. 2285). Each patient provided written informed consent prior to participation, and all clinical data were anonymized. To examine the metabolomics profile in CRSwNP patients, paired tissue specimens (NPs and normal nasal mucosa) were resected from eosinophilic CRS patients who underwent endoscopic sinus surgery in our department from April 1, 2020 to March 31, 2021. All enrolled patients were clinically diagnosed with eosinophilic CRS based on the JESREC scoring system. Exclusion criteria included patients undergoing or within 5 years of malignant tumor treatment, patients using oral steroid medication or antibody therapy for allergic diseases, such as bronchial asthma or atopic dermatitis, patients with autoimmune diseases, and other patients deemed inappropriate by the physician. The biological samples were stored at −80°C until analysis. Recurrence was defined as a worsening of sinonasal symptoms and regrowth of NPs observed during postoperative consolidation therapy with oral corticosteroids.

Sample preparation for metabolomics analysis

The sample preparation for the measurement of primary metabolites was described previously [1-3]. In brief, 500 μL of methanol was added to 7.5 mg of frozen tissue specimens. After homogenization for 2 min using a disposable pestle (Argos Technologies, Vernon Hills, IL, USA), the homogenate was centrifuged at 21,500 × g for 10 min at 4°C, and 150 μL of the supernatant was transferred to a new tube. Next, 250 μL of water and 500 μL of chloroform were sequentially added to the supernatant, followed by vortexing for 5 min. Subsequently, the mixture was centrifuged at 21,500 × g for 10 min, and 400 μL of the upper layer was applied to an Amicon Ultra 0.5 mL centrifugal filter (3 kDa molecular weight cut-off; Merck KGaA, Darmstadt, Germany). The filtrate was dried with a centrifugal vacuum concentrator (Taitec Corporation, Saitama, Japan), and the residue was dissolved in 200 μL of water.

Liquid chromatography/electrospray ionization–mass spectrometry (LC/ESI–MS)

The prepared samples were placed into a TORAST-H Bio Vial (Shimadzu, Kyoto, Japan) and analyzed using an LCMS-8060 MS system (Shimadzu) with a high-pressure LC system installed. To analyze the primary metabolites, the LC/MS/MS method package for primary metabolites (v.3; Shimadzu) was used. The ultra-high-performance LC conditions were as follows: Discovery HS F5-3 column (150 mm × 2.1 mm I.D., 3 μm particle size; Merck KGaA) with mobile phases A (0.1% formic acid in water) and B (0.1% formic acid in acetonitrile). The mobile phase B gradient was programmed as 0% (2 min), 25% (5 min), 35% (11 min), 50% (12.5 min), 50% (16 min), and 95% (17 min). The column oven temperature was 40°C.

Quantitative analysis of primary metabolites and pathway analysis

Following the LC/ESI–MS analysis, quantitative analysis of the primary metabolites in each specimen was performed using LabSolutions v.5.82 SP1 (Shimadzu). The data processing and molecular quantification were described previously [2, 3]. Briefly, data processing and molecular quantification were automatically performed based on the retention time and the area of the spectrum peak for each metabolite. To identify metabolites with significant changes in the polyp group compared with the normal nasal mucosa group among the CRSwNP patients, the normalized ion intensity ratio of each metabolite was calculated for both groups and compared. Mann–Whitney U tests were performed. Based on the primary metabolites with significant changes, a heatmap analysis and pathway analysis were conducted using MetaboAnalyst 5.0 (https://www.metaboanalyst.ca/).

Single-cell RNA sequencing analysis

Publicly available single-cell RNA sequencing data from the GSE276503 dataset were used to examine the metabolic gene expression profiles in CRSwNP. The dataset included NP samples (n = 15) and control inferior turbinate (IT) mucosa samples (n = 9) from CRSwNP patients. Raw data were downloaded and processed using the Scanpy (v.1.9.3) pipeline in Python. After quality control, normalization, and dimensionality reduction, cell clustering was performed using the Leiden algorithm. UMAP visualization was used to assess the distribution of cell populations. Cell types were annotated based on canonical marker genes, including markers for epithelial (e.g., basal cells, goblet cells), stromal (e.g., fibroblasts), and immune (e.g., T cells, macrophages) cell types. Marker-based dot plots and cluster-specific gene rankings were used to validate the annotation. To investigate metabolic remodeling, we defined gene sets related to four key metabolic pathways: the TCA cycle, glutamic acid metabolism, BCAA metabolism, and the tryptophan–kynurenine pathway. For each pathway, expression scores were computed by averaging the normalized expression values across genes

within the pathway. Violin plots were generated to compare the pathway scores between the NP and IT samples in representative cell types (i.e., basal cells, fibroblasts, and T cells). To complement these results, we calculated the differential expression (NP – IT) for each gene in each pathway and cell-type category and visualized the resulting data using heatmaps. This integrative approach enabled comparisons of metabolic activity in each cell type between non-polyp and polyp tissues, highlighting basal cell-specific transcriptional changes linked to TCA cycle suppression, glutamic acid re-routing, and kynurenine accumulation. The expression scores were derived from the averaged gene expression values per pathway per cell type.

Statistical analysis and classifier creation

GraphPad Prism (v.8.0) and MetaboAnalyst 5.0 were used for graph creation and statistical analysis. P-values were calculated using the Mann–Whitney U test to determine the statistical significance of specific molecules. Values of $p < 0.05$ were considered statistically significant. To examine the diagnostic accuracy of candidate biomarkers, receiver operating characteristic (ROC) curves were created, and the area under the curve (AUC) was calculated for each metabolite. BellCurve for Excel v.4.05 (Social Survey Research Information Co., Japan) was used to generate univariate ROC curves and to compare the AUC values. Metabolites with moderate accuracy (AUC > 0.8) were selected as candidate biomarkers.

References

1. Ashizawa K, Yoshimura K, Johno H, et al. Construction of mass spectra database and diagnosis algorithm for head and neck squamous cell carcinoma. Oral Oncol. 2017;75:111-9.
2. Iwano T, Yoshimura K, Watanabe G, et al. High-performance Collective Biomarker from Liquid Biopsy for Diagnosis of Pancreatic Cancer Based on Mass Spectrometry and Machine Learning. J Cancer. 2021;12(24):7477-87.
3. Kiritani S, Yoshimura K, Arita J, et al. A new rapid diagnostic system with ambient mass spectrometry and machine learning for colorectal liver metastasis. BMC Cancer. 2021;21(1):262.

Table S1. Patient characteristics.

	Gender	Age	Tissue eosinophil count per HPF [a]	Bronchial asthma	Recurrence within 6 months after surgery	JESREC [b] score	Total IgE antibody	Blood eosinophil %
Patient #1	F	58	100	(+)	(+)	17	694	14.6
Patient #2	F	78	100	(+)	(+)	15	58	7.7
Patient #3	M	55	80	(+)	(–)	15	283.3	6.5
Patient #4	M	80	70	(+)	(–)	15	62.1	8.3
Patient #5	F	56	380	(–)	(+)	14	120	10.4
Patient #6	M	45	285	(–)	(–)	15	1089.4	13
Patient #7	F	66	85	(+)	(+)	17	83	13.4
Patient #8	M	52	80	(+)	(+)	15	602	5.1
Patient #9	M	66	100	(–)	(–)	11	23.4	9.9
Patient #10	M	46	100	(–)	(–)	15	834.2	6.2
Patient #11	F	28	300	(–)	(–)	15	65	8.3
Patient #12	M	67	80	(+)	(–)	17	203.1	11.7
Patient #13	M	57	350	(+)	(+)	17	497.7	18

[a] HPF: high power field; [b] JESREC: Japanese Epidemiological Survey of Refractory Eosinophilic Chronic Rhinosinusitis Study.

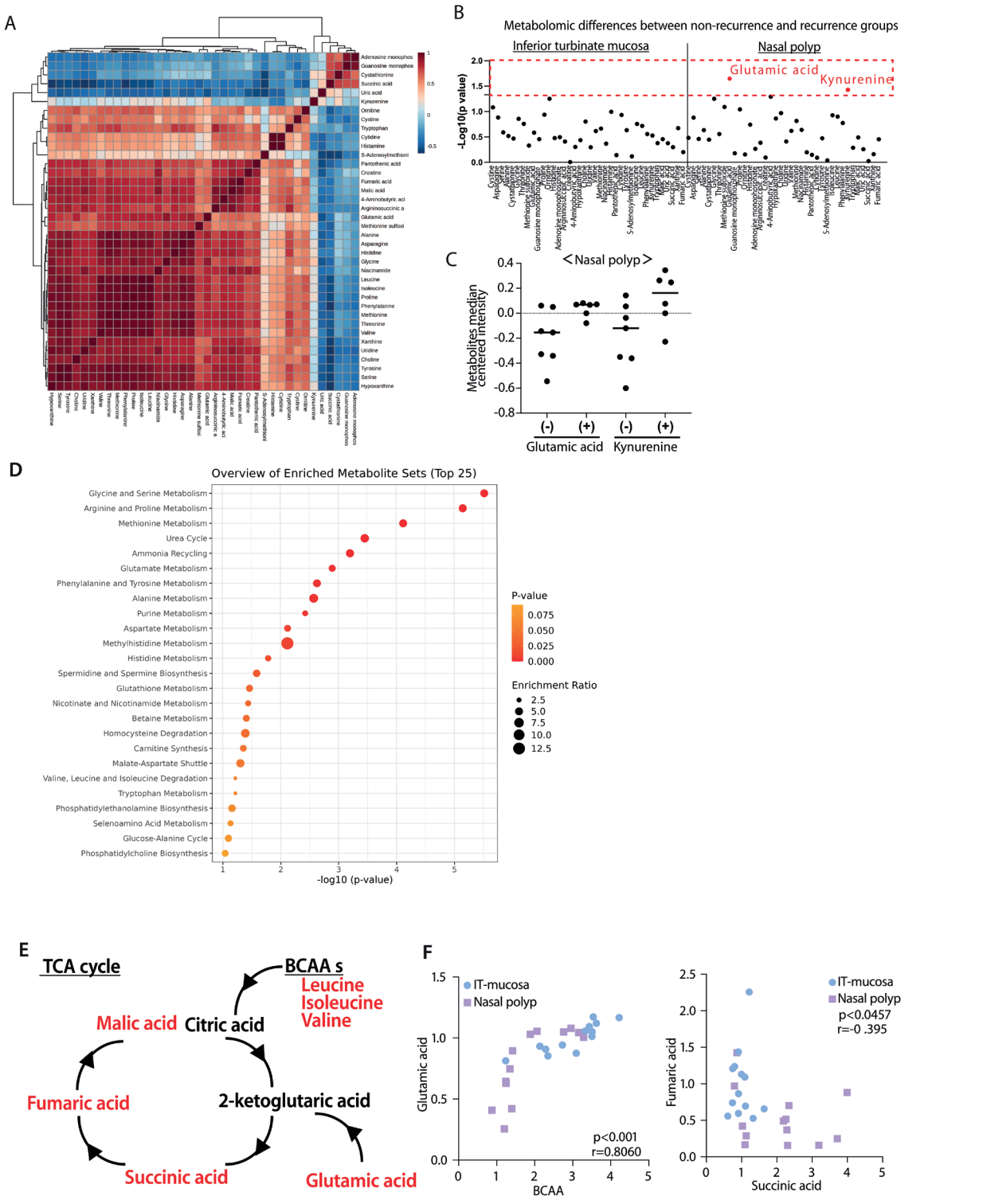

Figure S1. (A) Pearson correlation matrix among the 38 quantified metabolites in the inferior turbinate (IT) and nasal polyp (NP) tissues from CRSwNP patients. Each cell represents the correlation coefficient between a pair of metabolites. Red and blue indicate positive and negative correlations, respectively. (B) Correlation analysis of metabolite levels with postoperative recurrence. The x-axis represents individual metabolites, with IT–derived metabolites shown on the left and NP–derived metabolites shown on the right. The y-axis indicates log-transformed p-values for comparisons between recurrence and non-recurrence groups. Metabolites showing statistically significant differences are highlighted. (C) Glutamic acid and kynurenine levels in NPs from patients with/without recurrence (recurrence, n = 6; non-recurrence, n = 7). (D) Pathway enrichment analysis based on the 38 primary metabolites. The top 25 enriched pathways are presented, with the bubble color indicating the p-value and the size representing the enrichment ratio. (E) Metabolic scheme of the TCA cycle with glutamic acid and BCAA metabolism (F) Correlation analysis of glutamic acid and BCAAs (left) and succinic and fumaric acids (right).

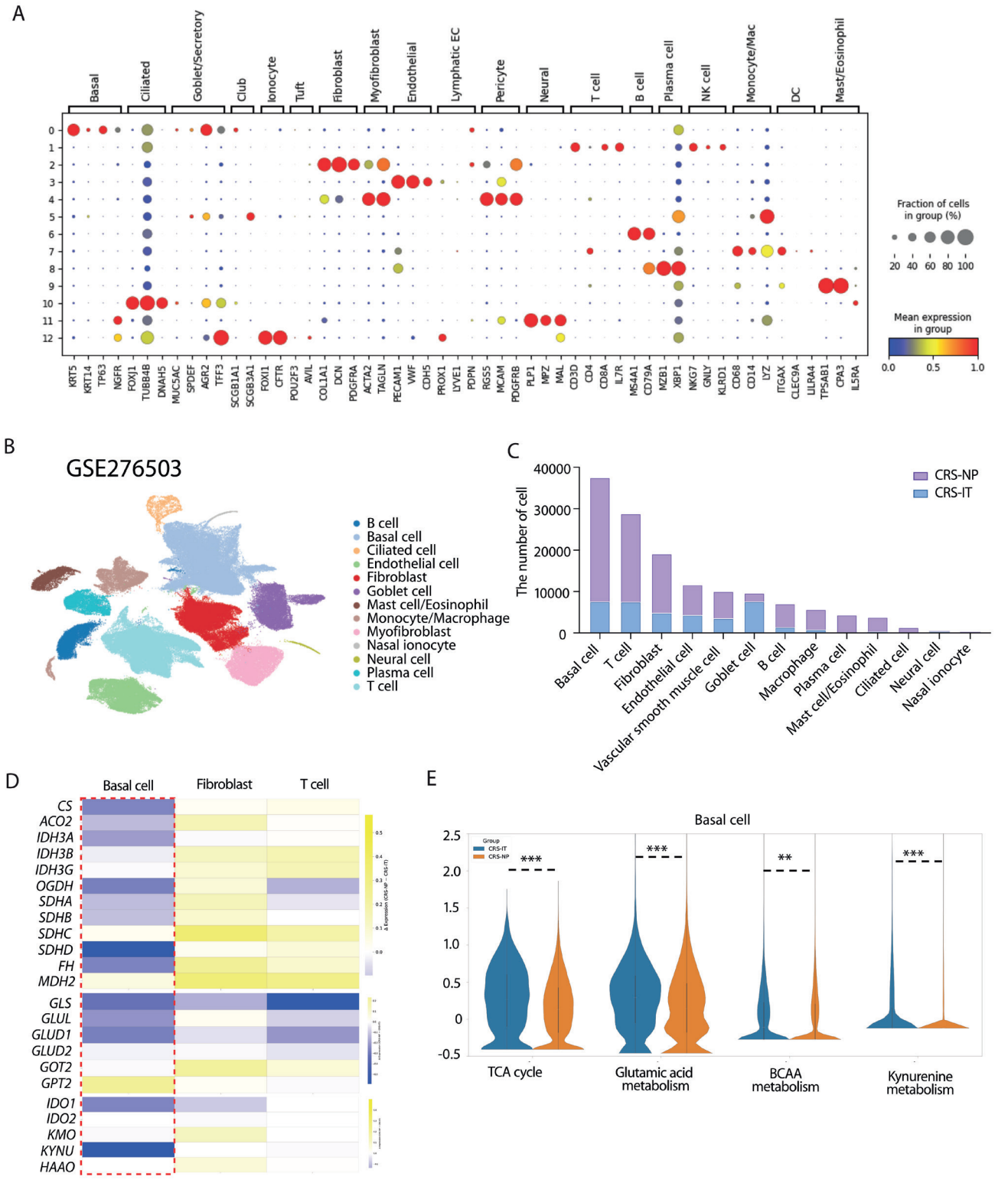

Figure S2. (A) Dot plot showing the expression levels of canonical marker genes used for cell type annotation. Red and blue colors indicate high and low expression levels, respectively. The size of each circle is proportional to the percentage of the cell fraction expressing the indicated genes. (B) UMAP visualization of single-cell transcriptomic data from inferior turbinate (IT) and nasal polyp (NP) of CRSwNP patients. (C) The number of each cell type in the ITs (blue) and NPs (purple). (D) Heatmap comparing the differential expression of metabolic genes in basal cells, fibroblasts, and T cells derived from the IT or NP tissues. Yellow indicates higher expression in NPs, while blue indicates higher expression in ITs. (E) Violin plots of pathway expression scores in basal cells. **p<0.01, ***p<0.001